STUDIES OF A FLAT WAKE ROTOR THEORY

H. C. Curtiss, Jr.
and
R. M. McKillip, Jr.

Department of Mechanical and Aerospace Engineering
Princeton University
Princeton, NJ 08544

Principal Investigator: H. C. Curtiss, Jr.

MAE Technical Report No. T1960

FINAL REPORT

NASA Research Grant NAG 1-1038
NASA Technical Officer: Dr. John C. Wilson
Mail Stop 286, Langley Research Center
Hampton, VA

October 1992

ABSTRACT

A computer code was developed at Princeton University under NASA Research Grant No. NAG 1-1038 to calculate the velocity components in the flow field near a lifting rotor based on the theory described in Reference 1, Chapters II and III. The user's guide for this code is given in Reference 2. The induced velocity components in the rotor flow field predicted by this theory are compared with experiment in References 1 and 3. Unfortunately, the sources of experimental data used for correlation in Reference 1 are either not well documented or not available. Reference 3 presents a thorough and detailed comparison. It appears that on balance, this relatively simple theory gives a reasonable prediction of the average induced velocities in a rotor flow field and is quite suitable for such applications as estimating the influence of the rotor wake on the tail surfaces of rotorcraft. The theory predicts that significant induced velocity components are present in all three flow directions in the wake at a lifting rotor. It should be noted however that there are few experimental measurements of the longitudinal and lateral induced velocity components in the rotor wake. This theory, known as the flat wake theory, is essentially the rotary wing analog of Prandtl's lifting line theory . The theory is described in this report and the development in Reference 1 is clarified. Calculations based on the theory are presented and compared with a modern free wake theory.

INTRODUCTION

Notes on Reference 1

Reference 1 presents in Chapters II and III a theory for the flow field in the vicinity of a lifting rotor based on the assumption that the vortices trailing from each blade move downstream in a path entirely determined by the path of the blade. Thus the resulting wake is flat, i.e., there is no downward motion, and there is no distortion. The path of the vortex line shed from a station on a blade is thus a cycloid which is simply the past motion of a point on the blade, (Figure 1). It seems that this assumption regarding the wake geometry is likely to be reasonable when the forward speed is high compared to the average induced velocity. The range of applicability proposed in Reference 1, (given in U. S. notation) is that

$$\frac{\sqrt{C_T}}{\mu} < .61$$

Momentum theory indicates that this corresponds to assuming that the theory applies at forward speeds greater than that at which the momentum value of the induced velocity is less than about twenty percent of the translational velocity.

It is further assumed that the wake composed of the cycloids shed from a single radial station on each of the blades may be smeared into a vortex sheet. This essentially corresponds to the assumption that the number of blades is large. The vortex

sheet wake that results from this assumption is shown in Figure 2. Inside the radius where the vortices are shed,there is vorticity in the direction of flight ('longitudinal vortices') and perpendicular to the direction of flight ('lateral vortices'). Outside this circle, i.e., in the wake there are only 'longitudinal vortices'. It may be noted that the longitudinal vortex sheet strength in the wake is not anti-symmetric (Fig 2.9) as would be the case for a symmetrically loaded wing. The implications of this result are discussed below.

The induced velocity components associated with this vortex sheet are calculated. Recall that this vortex sheet is associated with the vorticity shed at one radial station. The calculation of the complete flow field proceeds by assuming a circulation distribution along the blade, and then the contributions from the selected radial stations are superimposed suitably weighted by the magnitude of the circulation at the stations. The velocity components associated with one radial station are calculated in three parts.

First, the velocity components due to the lateral layer, within the circle of radius r are calculated (Chapter II,3.). The components of the flow field contributed by this element of the flow field consist of a downwash component and an in-plane component (parallel to the free stream). Above the plane of the wake, the in-plane component is in the direction of flight, and in the opposite direction below the rotor. This part of the flow

field gives the only in-plane induced velocity contribution, and generally indicates that there is a reduction in velocity at tail surfaces located below the rotor.

Second, the velocity components induced in a plane perpendicular to the direction of flight, passing through the rotor hub are calculated (Chapt II, 4). Using symmetry arguments, it can be seen that this flow field is that due at the upstream end of a flat rectangular wake stretching far downstream. Thus the velocity field calculated in this plane is just one half the far downstream value and this calculation may be thought of as a "far wake" model. Downwash and sidewash components are induced by this portion of the wake. The downwash field along the lateral axis passing through the rotor hub is shown in Figure 3 (Figure 2.21 of Ref. 1). Inside the radial station where the vortices were shed, the downwash is constant. However, note that outside this radius, the upwash is larger on the advancing side, than on the retreating side. There will also be a sidewash velocity, as shown in the figure which is induced by the vorticity distribution in the wake. Physically, the source of the asymmetry in the flow field is due to the symmetric component of the vorticity distribution in the wake (Figure 2.9 of Reference 1) as shown in Figure 3. Far downstream, considering the wake as two-dimensional in the Trefftz plane, the nature of the contributions to this flow field can be understood. The vorticity distribution in the wake can be split into two components one corresponding to the flow around a flat plate

perpendicular to the freestrem, without circulation (anti-symmetric). This corresponds to vorticity distribution in the wake of an elliptically loaded wing and produces a flow field that is symmetric, with no sidewash on the rotor centerline and equal upwash on either side. The second component is equivalent to the flow about a flat plate with circulation and corresponds to a symmetric vorticity distribution. This component produces the asymmetry in the flow field, with a higher upwash on the positive lateral axis and a sidewash to the left above the rotor as illustrated in Figure 3. This physical picture is useful in understanding the nature of the resulting flow field associated with a lifting rotor discussed below.

At this point in Reference 1, there is a digression to calculate the lateral distributions of downwash associated with an assumed circulation distribution along the blade. These downwash distributions in a plane perpendicular to the flight velocity, located at the rotor hub (one-half the value far downstream), are shown in Figure 2.22 for three circulation distributions. It is interesting to note that all of these relatively simple distributions, which are independent of azimuth, give a larger downwash on the advancing side than on the retreating side (Note reversal of the horizontal axis to account for the direction of rotor rotation of a Russian helicopter). The distribution for the constant circulation case is reproduced in Figure 4. Also shown is the sidewash distribution. It is interesting to note that the asymmetry in the flow field i.e.,

the larger downwash on the advancing side arises from the vortices shed from the root of the blade. The root vortices also primarily determine the sidewash flow field as indicated by the figure. Thus, the asymmetry in downwash noted in many experimental studies arises from the basic cycloidal nature on the wake.

Following this in Section 5, what may be called the near wake contributions are calculated, which make it possible to calculate the flow field velocities in planes perpendicular to the flow direction between the rotor hub and far downstream.

The details of all these calculations are given in Reference 1 and therefore are not repeated here.

The contributions of these three elements of the wake are then summed to give the three components of the induced flow field. Now given a circulation distribution along the blade, the three induced velocity components of the rotor flow field can be calculated.

Sample results are shown below. The method given in Reference 1 for determining the circulation distribution along the blade which is an input to the computer code that calculates the rotor flow field is described in Appendix I. The source of the values found in the computer code of Reference 2 is contained in Appendix 1.

DISCUSSION

Reference 2 presents the details of the computer code that

was written based on the developments in Reference 1 described above. Some typographical errors were noted in Reference 1, Chapter II, including: page 39, last term under radical in the expression for $\bar{Y}_y$ should be $(z-z_1)^2$; page 40, a minus sign is missing in the equation below equation (2.9), this velocity is equal to the negative of the integral; page 57, minus sign missing in equation (2.33), this velocity component is equal to the negative of the expression.

After the computer code was written it was checked with calculated results presented in Reference 1. After extensive checks on the code and derivation of the relationships in Chapter II, it was concluded that there are errors in the computed results shown in Figure 2.31 of Reference 1. The errors are primarily associated with the azimuth region near zero degrees. It is not clear what rotor blade characteristics are used for the calculated result shown in Figure 2.31, since the data and calculations presented in this figure are clearly the same as in Figure 2.34, however, the text indicates that the rotor blade in Figure 2.31 has no twist, while that in Figure 2.34 has 10 degrees of twist. Thus, it cannot be determined what circulation distribution was used for these calculations. Presumably, it is one of the distributions shown in Figure 3.3. However it was not possible to obtain agreement between the computer code of Reference 1 and the region near zero azimuth of Figure 2.31 for any reasonable circulation distribution.

Additional verification of the code was obtained by showing mathematically that the in-plane induced velocity components,

i.e., those parallel to the free stream do not vary with azimuth at a constant radius. The output of the computer code agrees exactly with this result (see Appendix II). This is also shown in Figure 2.33 where the computed velocity is the same at all five azimuth angles. In summary, it is concluded that the computer code of Reference 2 is an accurate representation of the flat wake model of Reference 1, and that there are small errors in Figure 2.31 of that reference.

The primary value of this approach to the difficult problem of the prediction of the induced flow field of the lifting rotor is its simplicity, which makes it possible to obtain physical insight into the rotor flow field, taken with the fact that it gives results that illustrate the general features of the rotor flow field. It clearly indicates the importance of other components of the rotor flow field in addition to downwash. The impact of the sidewash and downwash on rotorcraft stability and control are described in Reference 4. These effects taken with the predictions of the code indicate the desirability of obtaining additional data on the other velocity components of the rotor flow field.

Consider now the general nature of the flow field predicted by this code. The coordinate system used in the computer code is shown in Figure 5 and a sample output of the three components of the induced velocity in the vicinity of the horizontal tail location of a typical single rotor helicopter at an advance ratio of .2 are shown in Figure 6. These calculations use the cubic

circulation distribution of Reference 1 (See Appendix I) and are shown normalized by the momentum value of the induced velocity at the rotor hub. The distribution clearly shows the increased downwash on the advancing side of the rotor, the inplane wash is upstream, and the sidewash at this location is to the left since this location is below the rotor. The vertical distribution is shown in Figure 7. The inplane wash is upstream below the rotor and downstream above the rotor. The sidewash is to the right, or towards the advancing side above the rotor, and towards the retreating side below the wake.

These components are of significant magnitude, and will have a important influence of the aerodynamic characteristics of the horizontal, vertical tail, and tail rotor. Note for example that a high tail rotor will be operating in an upwash field, and a low tail rotor will operate in a downwash field, and there will be an effect of this flow field on the tail rotor power required. If the tail rotor is located above the wake,power required by the tail rotor may be appreciably reduced as noted in Reference 1. Additional effects of the sidewash on the stability and control of helicopters is considered in Reference 4.

In the next section some calculated results from the flat wake code are compared with a modern free wake code. In the free wake code the wake is allowed to distort as it leaves the rotor blade in a manner such that there are no forces exerted on the vortices (free wake model). There is, of course, no distortion in the flat wake model. In addition, the free wake

code closes the loop in the sense that the vorticity distribution in the wake is consistent with the vorticity distribution on the blade. This is not the case in the flat wake code where the circulation distribution on the blade is assumed.

Comparison with Advanced Free Wake Rotor Models

In order to successfully analyze the loads experienced by a helicopter in the presence of the main rotor wake it is necessary to accurately model the effect of the vortex wake of the main rotor. Over the past twenty years, a variety of computational rotor wake models have been developed, largely for application to problems concerning main rotor performance and airloads References 5, 6,and 7. Recently, a new approach to wake modelling has been developed that is superior in many important respects to previous work and has been successfully incorporated into analyses of rotorcraft interactional aerodynamics (Reference 8). This new approach involves using a force-free model of the wake over the full span of each rotor blade. Calculation of the induced velocity field based on this complex code will be compared with the simple code described in the first part of this report. This approach thus accounts for wake distrotion which is absent in the flat wake approach.

The fundamental building block of this analysis is the Basic Curved Element (BCVE), which is derived from the approximate Biot-Savart integration for a parabolic arc filament. When used in conjunction with a scheme to fit the elements along a vortex

filament contour, this method has a significant advantage in overall accuracy and efficiency when compared to the traditional approach, which involves the use of straight-line vortex segments. A theoretical and numerical analysis (Reference 9) has shown that free wake flows involving close interaction between filaments should utilize curved vortex elements in order to guarantee a consistent level of accuracy. The curved element method was implemented into a forward flight free wake analysis in Reference 10, featuring a single free tip vortex trailing from each blade, a model similar to many previous forward flight wake treatments. This model exhibited rapid convergence and robust behavior, even at relatively low advance ratio.

In many important forward flight conditions (particularly at high speed), the rotor wake structure can become very complicated, and wake models using a single free tip vortex are inadequate. On the advancing side, the generating blade may experience large spanwise and azimuthal load variations, including negative tip loading; the effects of such distributions will not be correctly captured by relatively crude single-vortex models. The new wake analysis methods described in References 10 and 11 seek to represent the important features of the resulting wake generated along the full span of the blade. Figure 8 shows the new full-span free wake generated by one blade of a four-bladed rotor at advance ratio 0.39. The curved elements are used to represent vortex filaments laid down along contours of constant sheet strength in the wake. The

skewed/curved filaments provide a natural representation of the free wake vorticity field, which simultaneously accounts for both shed and trailed vorticity. An additional advantage of the method is that it provides a visually meaningful representation of the wake since the filaments correspond to the actual resultant vorticity field. The vortex filaments leaving the blade in Figure 8 are all of constant strength, and each one is of equal value. For this reason, close spacing between filaments implies a strong net influence from that region of the wake, whereas a sparse spacing indicates a region of having little effect. The looping (or connecting) between outboard and inboard filaments is associated with changes in the maximum bound circulation on the blade. A strong root vortex structure is also evident. The actual aerodynamic environment experienced by the regions immersed in this complex wake structure can be inferred from Figure 8. From the standpoint of resolving the flow in the vicinity of the empennage, these wake geometry plots show a remarkably complicated incident wake structure that of course is not present in the flat wake theory.

This free wake model has been applied to the problem of the prediction of vibratory loads on the main rotor (Reference 11), the analysis of high-resolution flow fields for tail rotor aeroacoustics (Reference 12), and to the effects of the interaction of the rotor wake with downstream fuselage and empennage surfaces (Reference 8). This latter application is in a region of the flow field where it is interesting to compare

these two theories. In Reference 8, very encouraging correlation was found between measurements the time-average flow field downstream of an AH-64 wind tunnel model at advance ratio 0.28 and predictions made using the full-span wake model just described (see Figure 10, part of which was taken from Reference 13). In view of these results, it was naturally of interest to examine the correlation between the predictions made by the full-span free wake model and the flat wake model described above. The full-span model has been successfully applied for research on a variety of topics in rotor aerodynamics, but is on the whole too computationally demanding for routine use in studies of flight dynamics, for example. Thus, it is desirable to see if the flat wake representation captures the major features of the wake effect on empennage surfaces downstream of the rotor.

Sample calculations were performed using an isolated UH-60 main rotor at advance ratio 0.2, operating at a specified thrust coefficient. The shaft angle of attack and the blade pitch were set at values corresponding to the desired forward flight trim condition. In the current free wake analysis, a vortex lattice model of the blade is used, along with a relatively simple blade dynamics model featuring rigid flapping and one elastic bending mode. A trim routine is coupled to the blade dynamics analysis to ensure that the pitch control inputs to the blade are consistent with zero net hub moment.

For flow field computations, a measurement grid is set up downstream of the main rotor, and the predicted velocity field

is computed and stored at each time step. For these calculations, sixteen time steps per main rotor azimuth were used. Since the wake analysis starts assuming an undistorted, kinematic wake, typically several rotor revolutions of simulated time must elapse before the calculation reaches a repeatable steady state. Once such a state is achieved, the velocity field at the measurement grid is time-averaged and normalized; these results can then be directly compared with the flat wake predictions.

The first calculation undertaken here examined the UH-60 operating at a thrust coefficient of 0.007 and a shaft angle of attack of -5 deg. The plots in Figures 10 and 11 show the comparisons of downwash and sidewash predicted by the flat wake and free wake models at the vertical level corresponding to the horizontal stabilizer position. As is evident, the predicted velocity fields are qualitatively quite similar and also show considerable quantitative similarities except in the peak values on the advancing side. One possible explanation for this dissimilarity is the different treatments of the blade bound circulation in the two cases. The flat wake calculation assumes a simple cubic bound circulation distribution whose magnitude is proportional to the momentum theory value of downwash and which is invariant with azimuth angle. The free wake calculation computes the spanwise circulation distribution for each azimuth angle that satisfies the flow tangency conditions at the blade surface. Clearly, this could lead to substantially different

bound circulation distributions, which could in turn produce significant changes in the flow field downstream.

To quantify the differences in the bound circulation, the time-averaged circulation for the free wake calculation was calculated and is shown in Figure 12. The distributions show considerable differences near the root and the tip, and the peak level of average circulation is substantially lower in the free wake case than in the flat wake case. The flat wake value is roughly 15% higher than the free wake prediction; since the flat wake velocity field scales with the maximum bound circulation, reducing the flat wake input to match the peak spanwise level in the free wake calculation would improve the agreement considerably. The deviation of the bound circulation from the assumed cubic distribution would also effect the predicted velocity field; thus, it would probably be desirable to adjust the spanwise circulation distribution to be more representative of actual load distributions in follow-on applications of the flat wake model. Nonetheless, the agreement for this case (at relatively high forward speed) is quite encouraging, particularly the downwash in the immediate vicinity of the horizontal stabilizer position ($\bar{z}$ = -0.25 to 0.25).

An additional calculation was undertaken to compare the vertical distribution of sidewash experienced by the tail rotor and vertical tail for this same flight condition. The results for both the free wake and flat wake models are shown in Figure 13. Note that the free wake result does not display the symmetry of the flat wake case, though it does tend to reduce the peak

levels of sidewash that are observed. Also, though the vertical gradient of sidewash is steep even in the free wake case, it is somewhat "softened" relative to the abrupt jump evident in the flat wake results of Figure 7.

Based on this limited comparison, the results from the two approaches are quite similar, and he simple flat wake theory appears to capture quite well the average features of the flow field downstream of a lifting rotor.

SUMMARY

The flat wake model of Reference 1 shows reasonable agreement with a computationally intensive free wake model for the prediction of the flow field downstream of a lifting rotor. Other studies have shown that the free wake model agrees well with experiment. This and other studies show that the relatively simple flat wake model predicts the important features of the flow field behind a lifting rotor and shows fair to good agreement with experiment.

The difference between theory and experiment is related to the fact that the flat wake theory does not include any distortion of the wake, and also uses an assumed circulation distribution that is not consistent with the rotor blade geometry.

The simple nature of this flat wake theory, and the fact that it predicts important features of the wake should make it useful in studies of flight dynamics and interactional

aerodynamics and as a guide for experimental studies.

Additional experimental data, especially for the lateral and in-plane components of the induced velocities downstream of a rotor would be useful for further evaluation of this and other theories. While the downwash component is of primary importance in rotor aerodynamic studies, the flat wake theory indicates the importance of the other components as related to the effect of the main rotor on the tail rotor and tail surfaces.

REFERENCES

1. Baskin, V. E, et al: Theory of the Lifting Airscrew. (Mashinostroyeniye Press, Moscow, 1973.) NASA Technical Translation F-823, February 1976.

2. Wilson, J. C.: User's Guide for A "Flat Wake" Rotor Inflow/Wake Velocity Prediction Code, "Down". NASA TM 104139, AVSCOM Technical Report 91-B-016, November 1991.

3. Wilson, J. C.: Experimental Evaluation of a Flat Wake Theory for Predicting Rotor Inflow-Wake Velocities. NASA TM 4334, AVSCOM Technical Report 92-B-004, April 1992.

4. Curtiss, H. C., Jr. and Quackenbush, T. R.: The Influence of the Rotor Wake on Rotorcraft Stability and Control. Paper presented at the 15th European Rotorcraft Forum, Amsterdam, The Netherlands, September 12-15, 1989.

5. Scully, M. P.: Computation of Helicopter Rotor Wake Geometry and Its Influence on Rotor Harmonic Airload, Massachusetts Institute of Technology Aeroelastic and Structures Research Laboratory, ASRL TR 178-1, March 1975.

6. Egolf, T. A. and Landgrebe, A. J.: Helicopter Rotor Wake Geometry and Its Influence in Forward Flight, Vols., I and II, NASA CR 3726 and 3727, October 1983.

7. Sadler, S. G.: Main Rotor Free Wake Geometry Effects on Blade Air Loads and Response for Helicopters in Steady Maneuvers, NASA CR 2110 and 2111, September 1972.

8. Quackenbush, T. R. and Bliss, D. B.: Free Wake Prediction of Rotor Flow Fields for Interactional Aerodynamics, Proceedings of the 44th Annual Forum of the AHS, June 1988.

9. Bliss, D. B., Teske, M. E. and Quackenbush, T. R.: A New Methodology for Free Wake Analysis Using Curved Vortex Elements, NASA CR 3958, 1978.

10. Bliss, D. B., Dadone, L. U. and Wachspress, D. A.: Rotor Wake Modelling for High Speed Applications, Proceedings of the 43rd Annual Forum of the AHS, May 1987.

11. Quackenbush, T. R., Bliss, D. B. and Wachspress, D. A.: Preliminary Development of an Advanced Free Wake Analysis of Rotor Unsteady Airloads, Final Report to NASA/Ames under Contract NAS2-12554, August 1987.

12. Quackenbush, T. R., Bliss, D. B. and Mahajan, A.: High Resolution Flow Field Predictions for Tail Rotor Aeroacoustics,Proceedings of the 45th Annual Forum of the AHS, May 1989.

13. Logan, A. H., Prouty, R. W. and Clark, D. R.: Wind Tunnel Tests of Large- and Small-Scale Rotor Hubs and Pylons, USAAVRADCOM TR-80-D-21, April 1981.

APPENDIX I

Radial Distribution of Circulation

Nomenclature

a	blade lift curve slope (5.6)
χ	tip loss factor (.94)
μ	advance ratio (.15)
σ	solidity (.07)
ϕ	local blade pitch angle
ϕ_o	blade pitch angle .7R
$\Delta\Phi$	blade twist (10^0)
$\bar{\Gamma}_{cp}$	average circulation $\bar{\Gamma}_{cp} = 2 \int_{r_o}^{1} r\,\bar{\Gamma}\,dr$ (Eqn. 3.10)
$\bar{\Gamma}$	local circulation normalized by tip speed and radius
k	number of blades
$\tilde{b}$	undefined parameter ($\tilde{b} = 1$, untapered blades)
C_T	thrust coefficient (.012)

$$C_T \equiv \frac{2T}{\rho\ \pi R^2 (\Omega R)^2} = \chi\ \frac{k}{\pi}\ \bar{\Gamma}_{cp} \qquad \text{(Eqn. 3.9)}$$

$$\tilde{C} = \frac{1}{1 + \frac{8\mu}{a_\infty \sigma}}$$

(numerical values are those used in examples in Reference 1.)

Discussion

Chapter III of Reference 1 presents relationships based on blade geometry to estimate the average circulation distribution on a blade. The equations presented here are for zero angle of attack ($\alpha \rightarrow 0$).

The normalized circulation is given in equation 3.35 as

$$\bar{\Gamma} = \frac{\bar{\Gamma}}{\bar{\Gamma}_{cp}} = 4\mu \frac{\chi}{C_T} \tilde{C} \phi f(r) \qquad (3.35)$$

where

$$f(r) = r \left(\frac{r^2 + 0.5\mu^2}{r^2 + \tilde{C}_\mu{}^2}\right)$$

The rotor blade pitch is determined from equation 3.51. Note that this equation for the pitch of the blade at .7 radius gives the results in degrees

$$\phi_o^o = 21.8 \frac{C_T}{\sigma} (1.43 + \frac{\sigma}{\mu}) + .05 \Delta\phi^o \qquad (3.51)$$

Using the physical values for the parameters listed in the nomenclature, the pitch at .7R is,

$$\phi_o = 7.59^o$$

The local pitch is,

$$\phi_o = 14.59^o (1 - .685r)$$

Inserting the remaining parameter values in equation (3.35), the circulation distribution is,

$$\tilde{\Gamma} = (1 - 0.685r)\ r\ \left(\frac{r^2 + .011}{r^2 + .0055}\right)$$

Some constants were eliminated from this equation since the computer code normalizes the circulation.

If the blade is untwisted, the second term in the first parenthesis is not present and the remaining terms may be approximated as a linear function of radius,

$$r\left(\frac{r^2 + .011}{r^2 + .0055}\right) \cong .963r + .0411$$

This value in the untwisted case was multiplied by the quantity

$$4\mu \frac{\chi}{C_T}\ \tilde{C}\ \phi_o = 1.432$$

Recall that ϕ_o is different from the twisted case. Thus the result is,

$$\Gamma = .0589 + 1.378\ r$$

Note that it was not necessary to introduce the constant above since the computer code uses a normalized circulation.

It may be noted that the equations given above for circulation and blade pitch are somewhat inconsistent due to approximations made in equation 3.51.

The other distributions contained in Reference 2, referred to as a parabolic distribution in the code is suggested on Page 56 of Reference 1. It should perhaps more properly be referred to as a cubic distribution, and it does give the physically reasonable distribution that the circulation is zero at each end of the blade.

APPENDIX II

In-Plane Induced Velocity Component

The computer code showed that the in-plane induced velocity component is independent of azimuth when the circulation distribution is independent of azimuth. The following is the mathematical proof. The inplane velocity component arises only from the lateral vortices inside the circle of radius r. The expression for this induced component is given on P. 39 of Reference 1. The contribution of one radial station to this component is proportional to the integral,

$$I = \int_{-1}^{1} dz \int_{-\sqrt{1 - z^2}}^{\sqrt{1 - z^2}} \frac{dx}{[(x - x_1)^2 + y_1^2 + (z - z_1)^2]^{3/2}}$$

The displacements have been nondimensionalized by the radius ρ. Now, it will be shown that this integral is independent of azimuth. First convert to polar coordinates,

$$x_1 = r_1 \sin\psi_1 \qquad z_1 = r_1 \cos\psi_1$$

$$x = r \sin\psi_1 \qquad z = r \cos\psi$$

The integral becomes,

$$I(\psi) = \int_0^1 \int_0^{2\pi} \frac{r \, dr d\psi}{(r^2 + y_1^2 + r_1^2 - 2rr_1 \cos(\psi - \psi_1)^{3/2}}$$

Now we calculate the derivative of this integral,

$$\frac{\partial I}{\partial \psi_1} = 3 \int_0^1 \int_{o-\psi_1}^{2\pi-\psi_1} \frac{\sin\xi \, d\xi}{(r^2 + Y_1^2 + r_1^2 - 2rr_1 \cos\xi)^{3/2}} \; r^2 \, r_1 \, dr = 0$$

where $\xi = (\psi - \psi_1)$.

The inner integral is independent of ψ_1 and is in fact equal to zero due to the interval 2π. Therefore, the integral I is independent of azimuth locations ψ_1 in agreement with the computer code output.

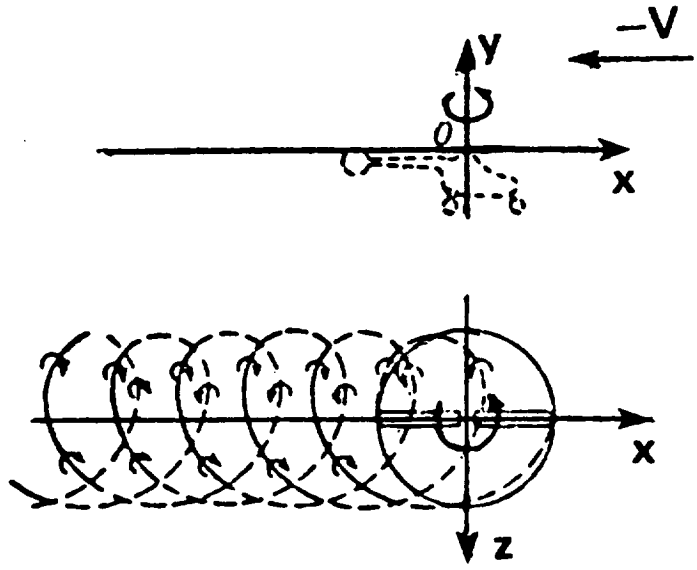

Figure 1: Cycloidal Flat Wake Geometry (two-bladed rotor, advance ratio = .25)

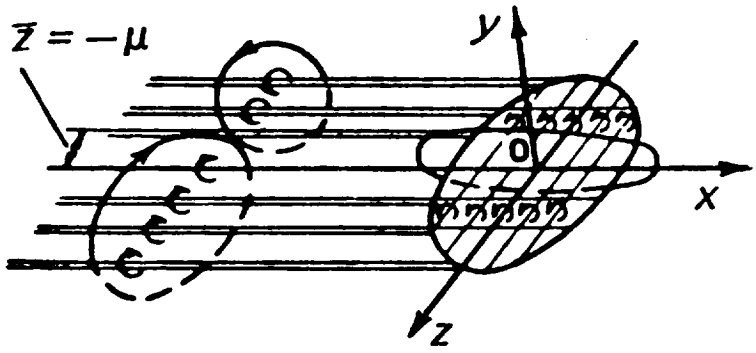

Figure 2: Vortex Sheet Wake. Equivalent to Cycloidal Wake of Figure 1

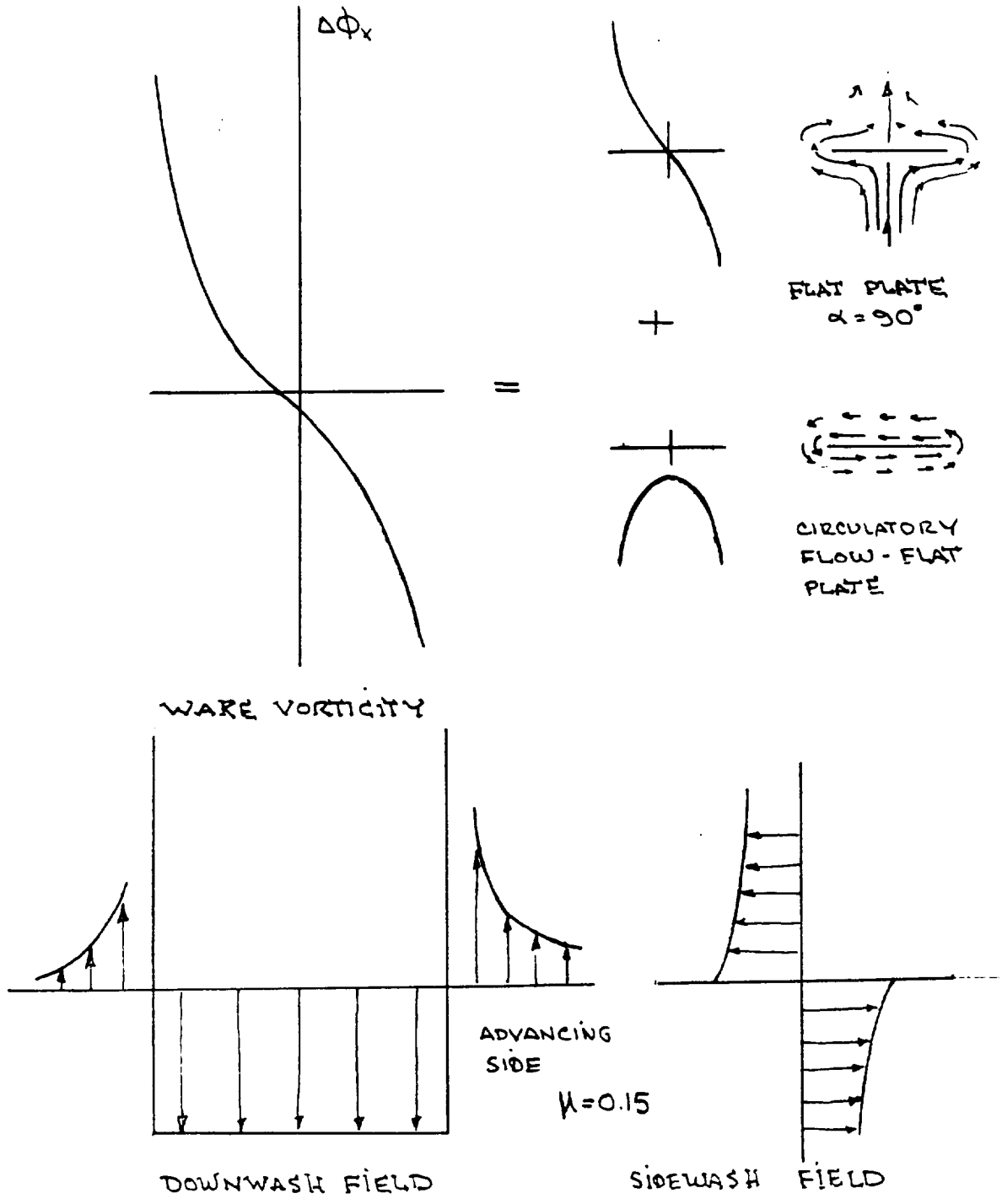

Figure 3: Flow Field Due to Unit Vorticity Shed at One Radius

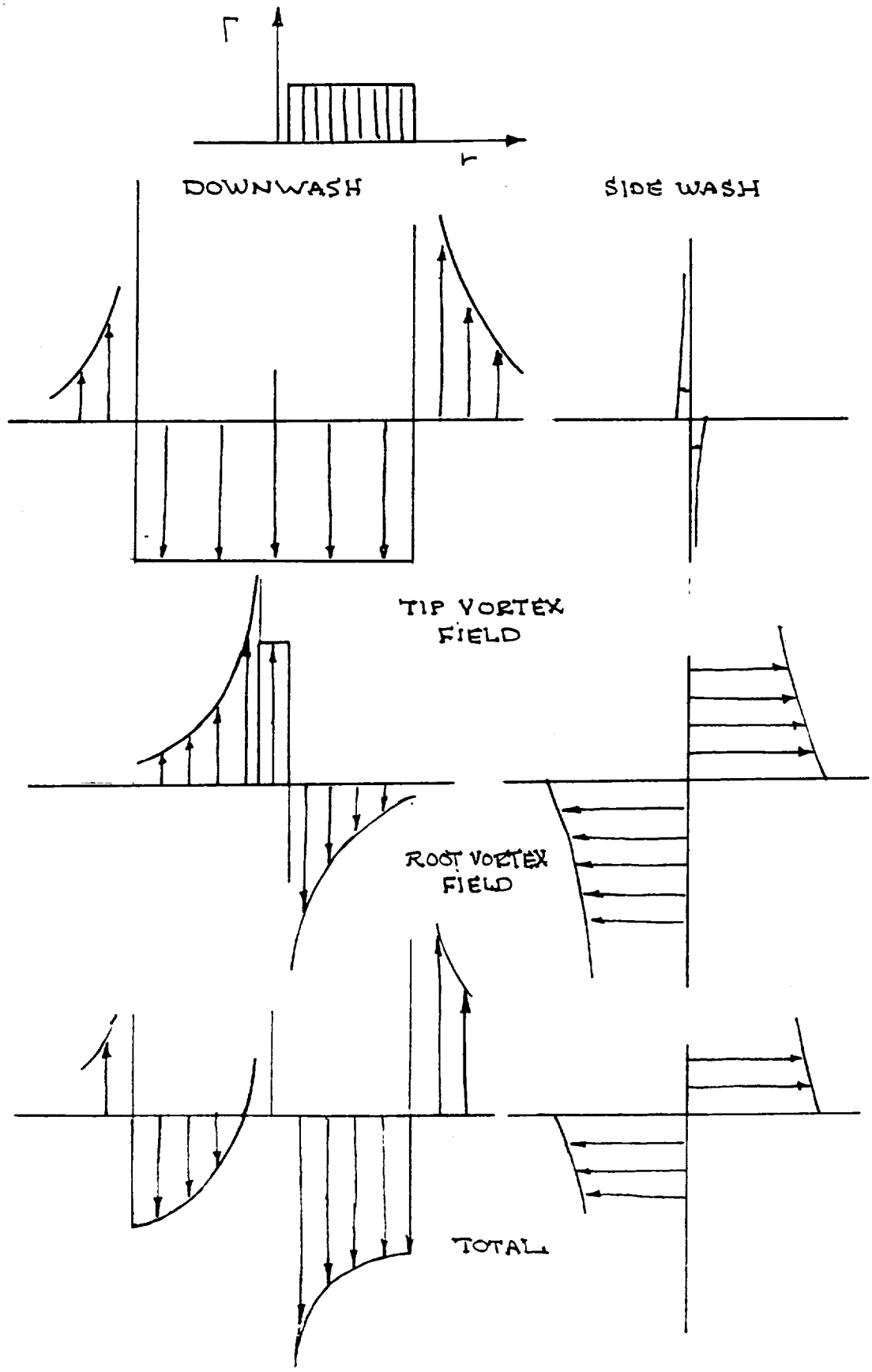

Figure 4: Contributions of Tip and Root Vortices to Rotor Flow Field

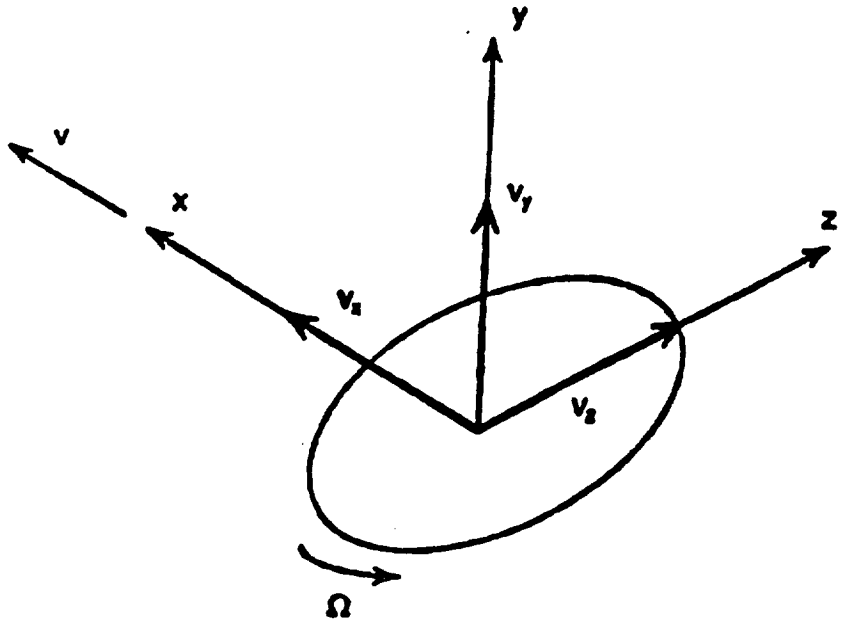

Figure 5: Coordinate System

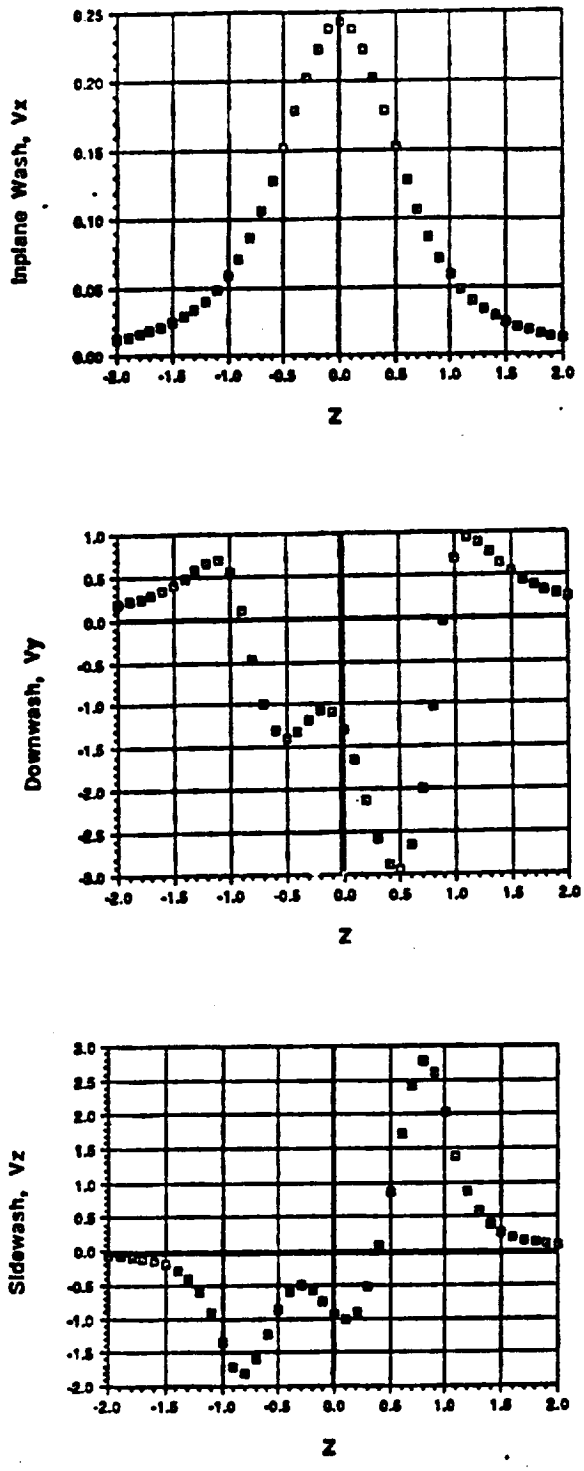

Figure 6: Flat Wake Lateral Distribution of Normalized Inducted Velocities Behind and Below a Lifting Rotor ($\bar{x}$ = - 1.1, $\bar{y}$ = -.22) Advance Ratio = .2) Circulation Distribution of Figure 12.

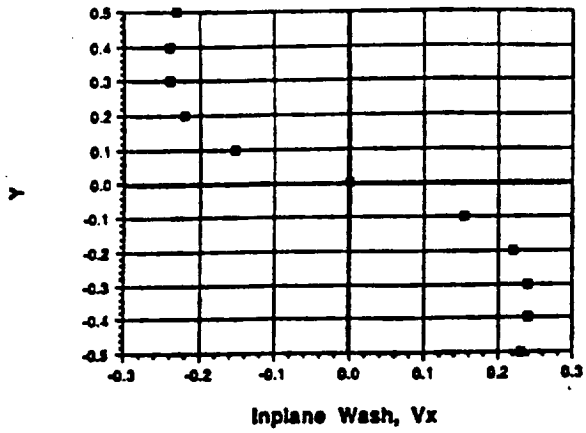

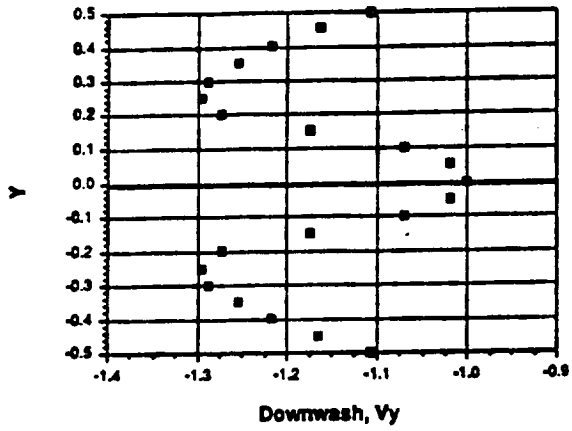

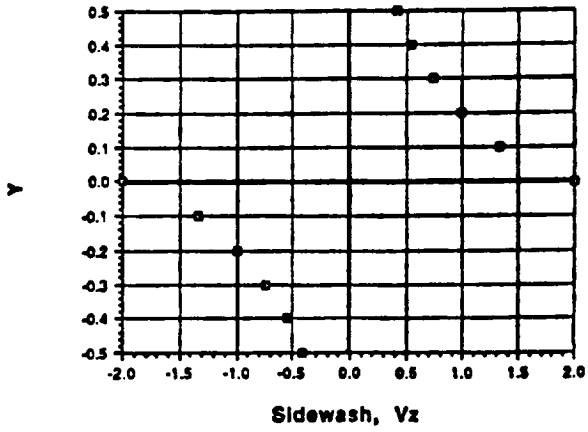

Figure 7: Distribution of Normalized Inducted Velocities Behind and Below a Lifting

Rotor ($x = -1.1$, $\bar{z} = -0.0$), Advance Ratio = .2) Circulation Distribution of Figure 12.

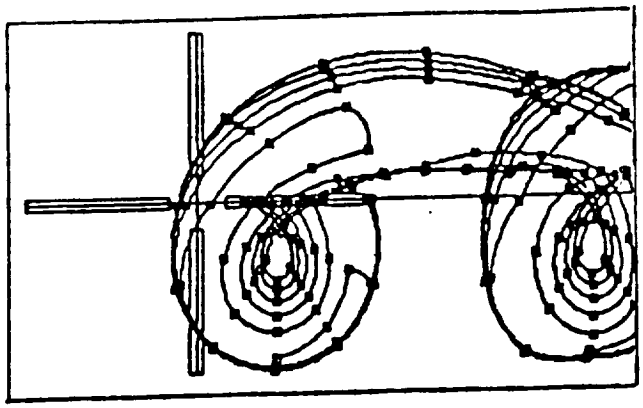

a) $\psi = 0°$

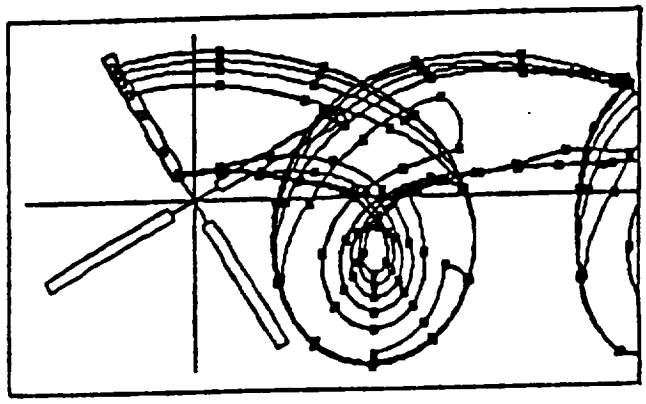

b) $\psi = 120°$

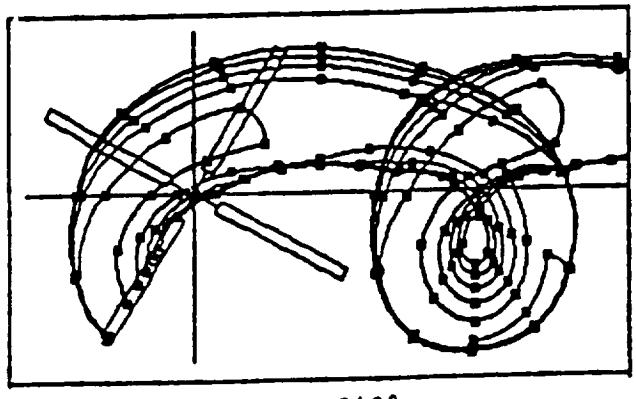

c) $\psi = 240°$

Figure 8: Full-Span Free Wake Geometry for a Four-Bladed AH-64 Main Rotor in Forward Flight At Advance Ratio 0.28

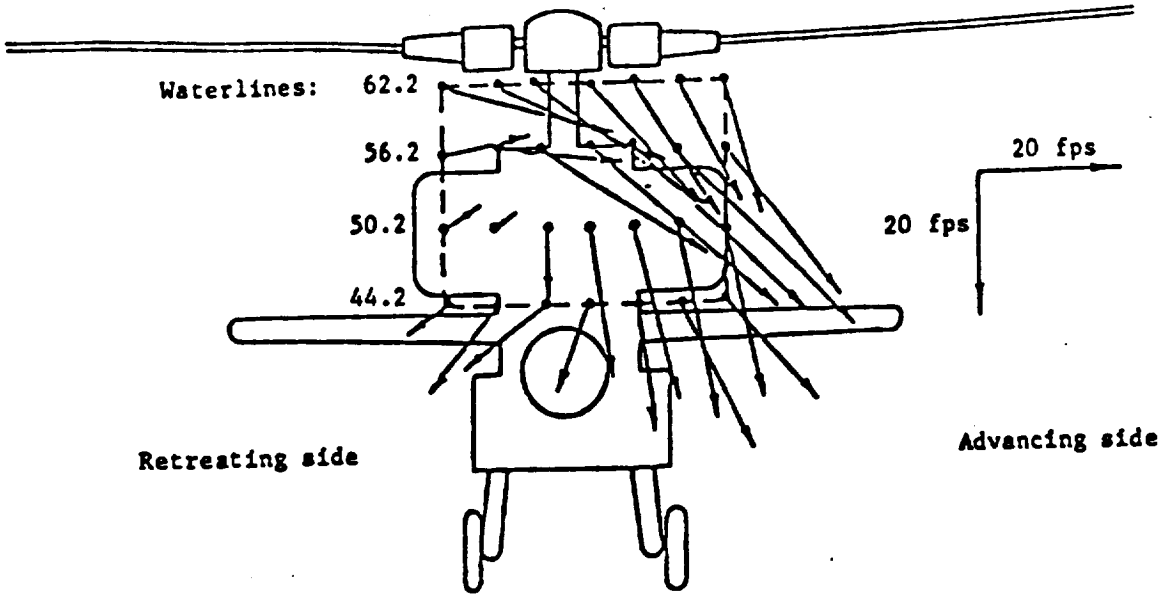

Figure 9: a) Crossflow Velocities for the AH-64 Wind Tunnel Model, ($\bar{x}$ = -1.3). Advance ratio 0.28 (from Reference 15

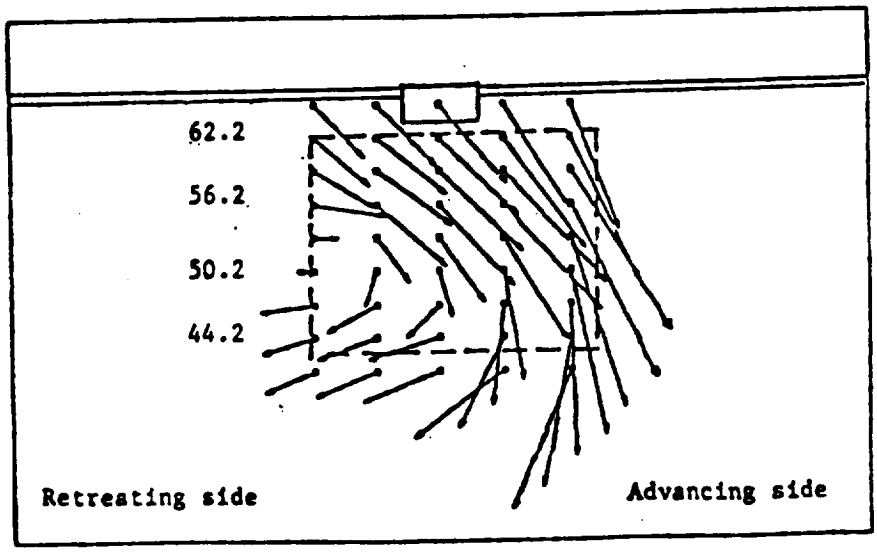

b) Free Wake Prediction of a) Identical Scales

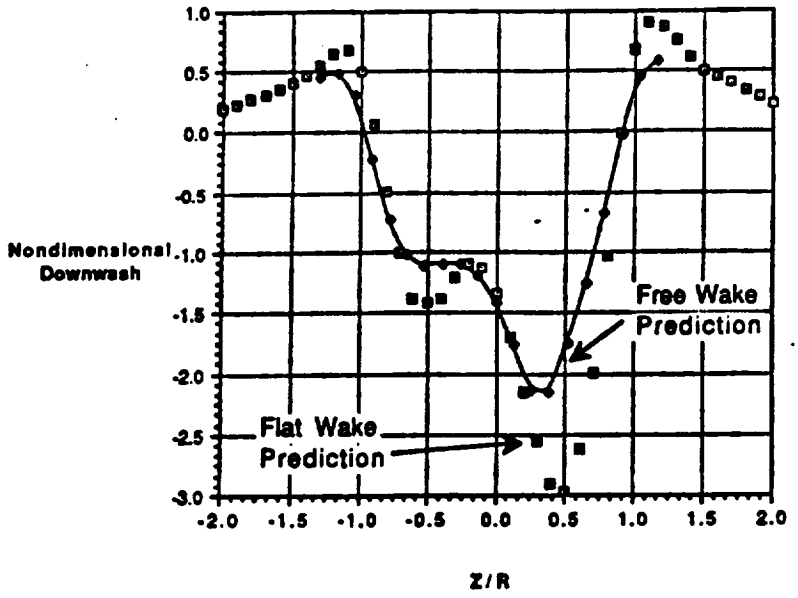

Figure 10: Comparison of Free and Flat Wake Predictions for Normalized Downwash at Horizontal Stabilizer Location UH-60. Advance Ratio = 0.2

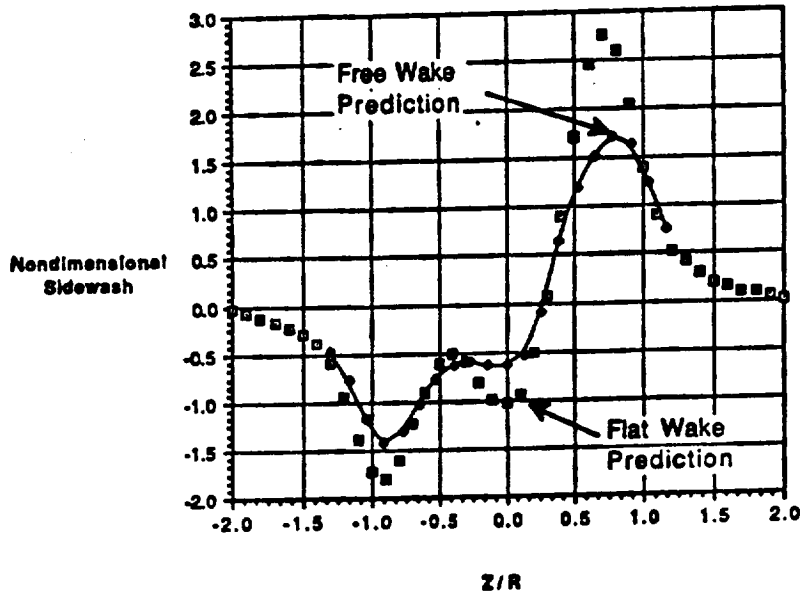

Figure 11: Comparison of Free and Flat Wake Predictions for Normalized Sidewash Distribution at Horizontal Stabilizer Location, UH-60, Advance Ratio = 0.2

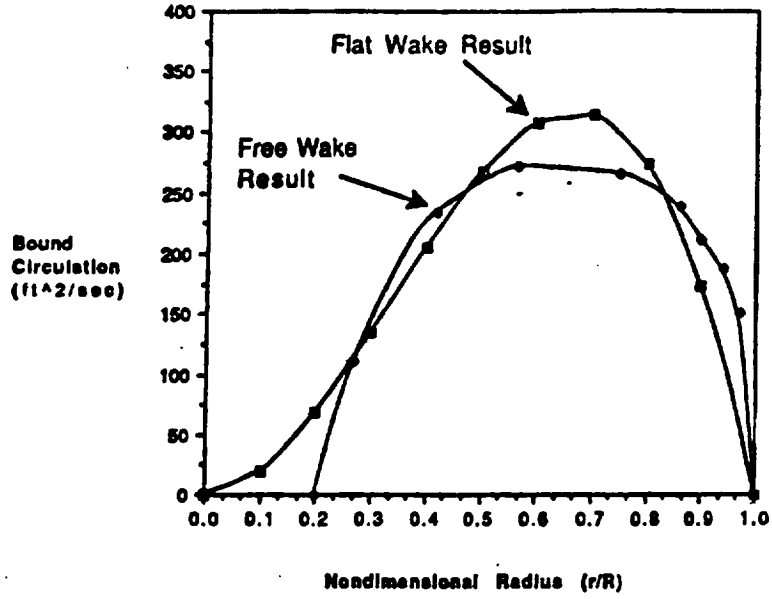

Figure 12: Comparison of Average Bound Circulation Distribution UH-60. Advance Ratio 0.2, Thrust Coefficient .007

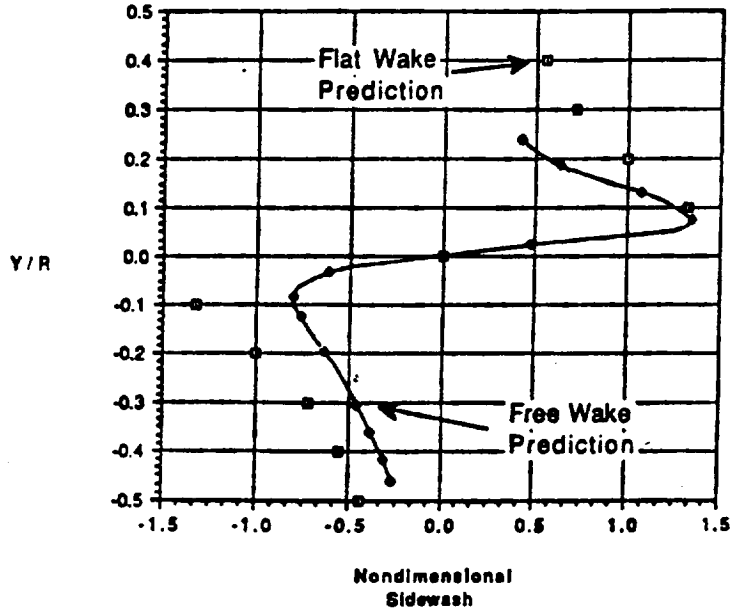

Figure 13: Comparison of Free and Flat Wake Prediction for Normalized Vertical Distribution of Sidewash, UH-60, Vertical Tail Location